Chemical Engineering Science, Vol. 44, No. 1, pp. 53–60, 1989.
Printed in Great Britain.

0009-2509/89 $3.00+0.00
Pergamon Press plc

SINTERING OF NASCENT CALCIUM OXIDE

ROBERT H. BORGWARDT
Air and Energy Engineering Research Laboratory, U.S. Environmental Protection Agency, Research Triangle Park, NC 27711, U.S.A.

(*Received* 12 *August* 1987; *accepted* 7 *June* 1988)

Abstract—The sintering rate of calcium oxide in a nitrogen atmosphere was measured at temperatures from 700 to 1100°C. CaO prepared from ultrapure $CaCO_3$ was compared with impure CaO derived from limestone and calcium hydroxide. $CaCO_3$ derivatives yielded an initial surface area of 104 m^2/g and the hydroxides, 76.7 m^2/g. The rate of surface reduction was independent of particle size between 2 and 20 μm, but strongly dependent on temperature and impurities. Impurities increased the rate of sintering at a given temperature and reduced the activation energy. The model of German and Munir (*J. Am. Ceram. Soc.*, **59**, 379–383, 1976) correlates the kinetics of surface reduction and identifies lattice diffusion as the mechanism of solid transport. Porosity declined logarithmically with time during the intermediate stage of sintering.

INTRODUCTION

Sintering is the mechanism by which solid particles coalesce when heated at temperatures below their melting point (m.p. of CaO = 2500°C). This paper concerns the sintering that occurs between the micrograins which comprise a porous particle produced by thermal decomposition of a $CaCO_3$ or $Ca(OH)_2$ particle. As coalescence of the micrograins progresses, the specific surface area and porosity of the particle are reduced, larger but fewer grains being ultimately formed. Sintering has been the subject of extensive experimental and theoretical study in the field of metallurgy and is known to be a solid-state phenomenon brought about by the force of surface tension (Rhines and DeHoff, 1984) such that the variations in curvature from point to point give rise to fluxes of matter (Johnson, 1980). The transport of matter that must occur during grain fusion and growth is effected by plastic flow and/or three types of diffusion: surface, grain boundary, or lattice.

The changes in surface area and porosity that accompany sintering affect the reactivity of a solid with fluids—a subject of interest to chemical engineers. Mathematical models that describe the reaction of solids with gases are becoming increasingly rigorous for application to a given solid structure. In many cases, high temperatures are required to achieve acceptable reaction rates and, because of sintering, the structure cannot be assumed constant. In the particular case of interest here, the sintering kinetics must be known in order to establish the initial surface area, or boundary conditions, for application of gas–solid reaction models.

Similarities between sintering and diffusion-controlled reactions

In addition to the inherent relationship between sintering and reactivity of solids, there is evidence that the sintering mechanism of CaO is fundamentally related to the transport process occurring in some—perhaps many—of its reactions with gases that form a solid product. Due to its technological importance, sulfation is the most thoroughly studied reaction of this type. Sotirchos and Yu (1985) have shown CaO sulfation to be controlled by diffusion in the product layer. Bhatia and Perlmutter (1981) propose that the diffusion occurs by a solid-state ionic transport process. Experimental studies of the effect of temperature and surface area on this reaction support that hypothesis (Borgwardt and Bruce, 1986), the evidence consisting of: (1) a high activation energy, 36.6 kcal/mol, that cannot be accounted for by gas phase diffusion; and (2) a greater sensitivity to specific surface area than expected for chemical reaction control. Similar characteristics were observed for the CaO reactions producing $CaSO_3$ (Borgwardt *et al.*, 1986) and CaS (Borgwardt *et al.*, 1984). An ionic diffusion mechanism is also thought to control the later stage of the reaction producing $CaCO_3$ (Bhatia and Perlmutter, 1983).

The nature of the diffusion process occurring in the product layer during reaction, and its relation to sintering, is further revealed by the effects of impurities and additives. Measurements of product layer diffusivities for the sulfation of CaO of varying purity show higher values for CaO derived from limestones than those prepared from pure $CaCO_3$ (Borgwardt *et al.*, 1987). Likewise, the addition of small amounts of certain salts is found to enhance sulfation (Slaughter *et al.*, 1986) especially when added to presintered CaO (Borgwardt *et al.*, 1987). The most effective of these salts contain cations that have a different valence than Ca^{2+}; such as Li^+, Na^+, Cr^{3+} and Mo^{3+}. These ions, when incorporated into a $CaSO_4$ or CaO lattice, produce defects that mediate solid-state diffusion, and their observed effects are therefore consistent with the hypothesis that diffusion through the product layer occurs by ionic transport. Similar effects of such aliovalent foreign ions are observed on CaO sintering, which suggests that its mechanism is related to that of product layer diffusion. One purpose of this study is to obtain information about the sintering mechanism that may further elucidate both processes.

From the standpoint of its physical structure, the reactivity of a solid is expected to depend on the specific surface area and porosity. The former affects rate, the latter affects both the accessibility of the internal surface to reactants diffusing in the gas phase and the amount of reaction product that can accumulate on the interior particle surface—and thus the ultimate conversion when solid products are formed.

Nascent CaO is defined here as that produced by the rapid decomposition of small, dispersed particles of $CaCO_3$ or $Ca(OH)_2$—a process yielding the maximum initial surface area (Borgwardt, 1985). The sintering and sulfation kinetics of nascent CaO are of current practical importance as they relate to pollution control technologies being developed to reduce acid rain by injecting limestone or hydrated lime into boiler furnaces (Lachapelle, 1985). These SO_2 sorbents are most effective at injection temperatures of 1040–1180°C (Beittel *et al.*, 1985) but rapidly lose the surface area associated with their reactivity (Cole *et al.*, 1985). In order to apply existing sulfation models to this process, sintering kinetics must be taken into account in terms not only of temperature but also of gas phase composition, since both CO_2 and H_2O in flue gas are known to accelerate CaO sintering. This paper is concerned specifically with the effect of temperature and time in the absence of CO_2 and H_2O as a first step in defining the overall process of surface area reduction in a flue gas atmosphere.

SINTERING MODEL

A standard two-sphere model of sintering particles was used by German and Munir (1976) to develop a kinetic relationship for surface area reduction. That model assumes that the grains have an initial spherical shape with multiple points of contact between adjacent grains. As sintering begins, a connecting neck forms at each point of contact and grows in diameter as matter is transported to the neck region under the influence of its curvature gradient. The transport of matter necessary for neck growth occurs by one of four possible mechanisms. The specific surface area is reduced by an amount proportional to the neck diameter and the number of initial contact points between grains. The following generalized expression was derived for this process:

$$\left(\frac{S_o - S}{S_o}\right)^{\gamma} = K_i t \qquad (1)$$

where S_o is the initial specific surface area, S is the specific surface at time t, and K_i includes the diffusion coefficient (a function of temperature), surface tension, and other constants. The exponent γ has unique values for the different transport mechanisms, which are: plastic flow, $\gamma = 1.1$; lattice diffusion, $\gamma = 2.7$; grain boundary diffusion, $\gamma = 3.3$; and surface diffusion, $\gamma = 3.5$. The German–Munir model can thus be used to identify the mass transport process via the kinetics of the specific surface area reduction. It was successfully applied to describe isothermal sintering kinetics of Al_2O_3, ZnO, Fe_2O_3 and TiO_2; in each case, the transport mechanism deduced from the evaluation of γ agreed with the mechanism established by other experimental methods. The assumptions on which eq. (1) is formulated are valid to a 50% reduction in surface area, at which neck overlap occurs and other surface reduction processes may become dominant. The exponent is also slightly dependent on the grain coordination number which may change with particle density.

EXPERIMENTAL

CaO was prepared from $CaCO_3$ by decomposing 25-mg samples in a differential reactor which is described elsewhere (Borgwardt *et al.*, 1986). Each sample was dispersed in quartz wool (*ca* 50 mg at 1.02 m^2/g surface area) and inserted in the stagnant reactor at 700°C. After a 2-min heatup period, calcination was begun by initiating nitrogen flow through the reactor at 20 l/min. Nitrogen of requisite purity was obtained from a liquid-N_2 tank. Calcination was continued for 3.5–10 min, depending on the $CaCO_3$ particle size. The resulting CaO sample was transferred (in *ca* 6 s) to an identical reactor at a higher temperature for sintering. Nitrogen flow was maintained through this reactor at 6 l/min. At the conclusion of the prescribed sintering period, the sample was withdrawn, cooled under flowing nitrogen, and transferred (including the quartz wool) to a BET flask. Fourteen such runs were composited and weighed for surface area analysis which was carried out by N_2 adsorption at 77 K using the multi-point BET method. The CaO was subsequently extracted from the flask with dilute HCl and titrated with EDTA for determination of the actual CaO weight (entrainment loss in the reactor was 0–20%, depending on particle size). The surface area of the quartz wool was subtracted to obtain the final value of the CaO specific surface area.

CaO was prepared from $Ca(OH)_2$ by the same procedure with the exception that no heatup period was used for calcination: because of the lower decomposition temperature of hydroxide, these samples were inserted in the reactor at 700°C with nitrogen flowing. Experiments which varied calcination time showed the surface area to be fully developed within 5 min and this period was used for all hydroxide calcinations.

The small sample size was used for two reasons: (1) to permit the decomposition reaction to proceed in a "differential" manner (i.e. the CO_2 is diluted and swept away to minimize its catalytic effect on sintering during the calcination step); and (2) to minimize the time required for temperature equilibration after transfer to the sintering reactor.

Because the sintering data are to be used for practical application involving impure CaO derived from limestones, those materials were the principal source of CaO for this study. The limestone was Fredonia White, BCR 2061, containing 96% $CaCO_3$. This is

one of several that have been characterized in detail by Harvey (1971). It was pneumatically classified into several narrow particle size fractions. Since the effect of impurities was an important object of investigation, a second source of CaO was evaluated for comparison. This material was ultrapure $CaCO_3$ (J. T. Baker Chemical Co., Ultrex) with total impurities certified at less than 200 ppm. It consisted of 10-μm crystals fused into agglomerates of about 80 μm.

The hydroxide used was also a commercial material, produced from Michigan Presque Isle limestone. Those tests were supplemented by sintering measurements with analytical grade $Ca(OH)_2$ (Fisher Scientific Co.) as a reference material. The latter was not pure by strict standards, containing more than 1 wt % of other constituents.

Porosity was of necessity measured with larger, 250-mg, samples which were not dispersed in quartz wool. Composites (800-mg) of these sintered samples were analyzed by nitrogen adsorption/desorption to determine poresize distribution and total pore volume. These measurements were made with a Micromeritics Digisorb analyzer. Pore volumes were determined by N_2 condensation at a relative pressure approaching the saturation pressure so that the largest possible pore sizes were included. At the relative pressure of 0.99, where these measurements were made, the Kelvin equation predicts that pores up to 0.19 μm in diameter will be filled. Most of the intraparticle pores are thus accounted for while excluding inter particle voids.

RESULTS

As pointed out by German and Munir, a critical step in the application of eq. (1) is the evaluation of S_o. The initial surface area was therefore measured repeatedly with the results summarized in Tables 1 and 2. The data show no clear dependence on the purity or particle size of the starting materials; therefore, an overall mean value of 104 m^2/g was used for all calculations involving $CaCO_3$ derivatives and 76.7 m^2/g for the $Ca(OH)_2$ derivatives. The latter value is based on measurements from a number of different types of hydroxides, identified in Table 2, including one prepared from the same limestone as used for carbonate testing.

Table 1. Data used to evaluate the initial surface area of CaO from carbonate precursors

Material†	Replicate S_o measurement (m^2/g)	Mean S_o (m^2/g)
Pure $CaCO_3$	112	104
	102	
	103	
	101	
Limestone, 2 μm	99.5	102
	96.9	
	111	
	99.6	
Limestone, 10 μm	103	106
	112	
	104	
	105	
Overall mean and probable error = 104 ± 1		

†Calcined at 700°C, no sinter.

The rate of surface area reduction in CaO prepared from pure $CaCO_3$ is shown in Fig. 1 at three sintering temperatures. Within the limits of strict validity of eq. (1), the broadest applicable range of ΔS is obtained at 1000°C; these data were therefore used for the initial estimate of γ. The minimum total deviation from eq. (1) was obtained with $\gamma = 3.0$, which yields the curve shown in Fig. 1 for 1000°C.

Figure 2 shows the rate of surface area reduction in CaO derived from limestone. Again, the exponent for eq. (1) was estimated by fitting the widest range of ΔS values that comply with the 50% limits which, in this case, are 900 and 800°C sintering temperatures. Values of $\gamma = 2.3$ and 2.8, respectively, yielded the best fit with these data.

Table 2. Data used to evaluate the initial surface area of CaO from hydroxide precursors

Material	Source	S_o of CaO (m^2/g)†
Commercial $Ca(OH)_2$	Presque Isle, Michigan	78.3
Commercial	Presque Isle (replicate)	80.0
Commercial	Marblehead, Pennsylvania	79.6
Analytical grade	Fisher Scientific Co.	76.5
Analytical	Fisher (replicate)	74.5
Analytical	Fisher (replicate)	73.6
Laboratory preparation	Fisher, calcined and rehydrated‡	74.7
Laboratory preparation	2 μm limestone, calcined and hydrated‡	76.0
	Overall mean	76.7
	Probable error	±0.6

†All materials calcined at 700°C, no sinter.
‡Three grams calcined for 180 min at 980°C (S of CaO = 3 m^2/g); slaked in water and dried in N_2, then recalcined at 700°C.

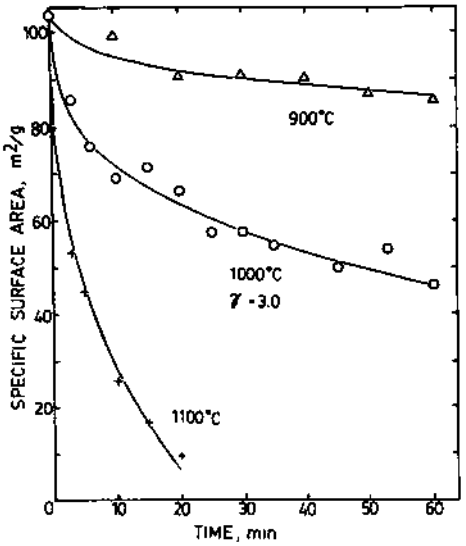

Fig. 1. Surface area reduction in pure CaO.

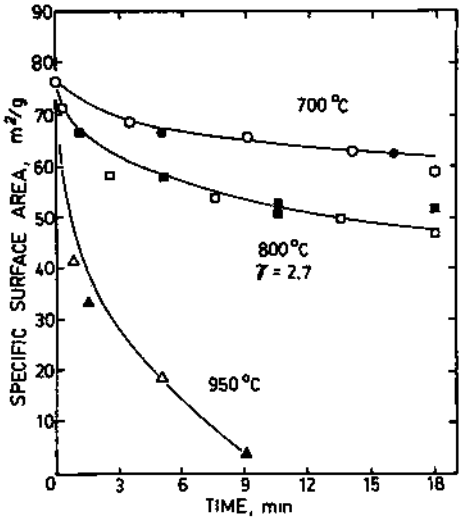

Fig. 3. Surface area reduction in hydroxide-derived CaO. Open symbols are Presque Isle commercial grade, closed symbols are analytical grade.

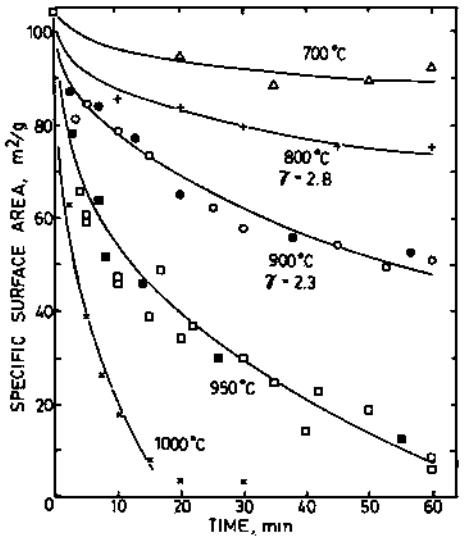

Fig. 2. Surface area reduction in limestone-derived CaO. Particle size = 2 μm, except for: (●) = 10 μm, and (■) = 20 μm.

The mean value of γ obtained from the above measurements, 2.7 ± 0.3, is in closest agreement with the mechanism of lattice diffusion. The range of validity of eq. (1) was tested by fitting the remaining data using $\gamma = 2.7$, the results of which are shown by the other curves in Figs 1 and 2. It is apparent that the German–Munir model adequately correlated the surface area reduction in nascent CaO to ΔS values exceeding 90%. The average deviation of the 51 limestone data of Fig. 2 (with $\gamma = 2.7$) is 3.2 m^2/g over this range.

CaO derived from $Ca(OH)_2$ gave the results shown in Fig. 3. The best fit of eq. (1) occurred with $\gamma = 2.7$ at each of the three sintering temperatures. These data corroborate the results obtained with carbonates and indicate that the same sintering mechanism is operative in both materials.

Table 3 summarizes the γ values obtained from all the data of Figs 1–3. They yield a mean value of $\gamma = 2.5$ for the seven estimates made from curves within the ΔS range of 0–0.55 and $\gamma = 2.7$ for all curves, where ΔS reaches 0.97 at the highest temperatures.

Since eq. (1) (with constant γ) correlates the S vs t responses within experimental error at all temperatures studied, the sintering rate constants, K_i, determined by the above procedure can be used to evaluate the temperature effect. For diffusion-controlled transport, the coefficient of diffusivity increases with temperature according to

$$D = D_o \exp(-E/RT)$$

and K_i should therefore follow the Arrhenius relationship. Figure 4 is such a plot, with K_i values determined by the best fit of eq. (1) to the data of Figs 1–3 with $\gamma = 2.7$.

Measurements of porosity are shown in Fig. 5 for 2-μm CaO particles sintered for 15 min at different temperatures. Below 900°C, the porosity remained nearly constant at a maximum value of 48%. During this period, the pore size distribution consisted of micropores smaller than 60 Å and macropores having a mean diameter of 170 Å. The latter comprised most of the total pore volume. Voids up to 300 Å, presumably fissures, were also present. At 950°C, few micropores remained. The mean diameter of the macropores was constant at 170 Å well into the final stage of sintering at 1000°C.

DISCUSSION

Surface area reduction

Comparison of the sintering rates of pure and impure CaO derived from $CaCO_3$ lends further support to the lattice diffusion mechanism deduced from

Table 3. Evaluation of γ from sintering data of Figs 5–7

CaO precursor	Sinter temperature (°C)	No. of data	ΔS range (%)	γ for best curve fit
Pure $CaCO_3$	900	5	16	2.0
Pure $CaCO_3$	1000	11	55	3.0
Pure $CaCO_3$	1100	5	94	3.1
Limestone	700	4	14	2.2
Limestone	800	5	29	2.8
Limestone	900	15	54	2.3
Limestone	950	22	93	3.2
Limestone	1000	6	97	2.9
Hydroxide	700	5	19	2.7
Hydroxide	800	10	38	2.7
Hydroxide	950	4	94	2.7
	Mean and standard deviation of $\bar{\gamma}$ for seven estimates, $0 < S < 0.55$			2.5 ± 0.1
	Mean and standard deviation of $\bar{\gamma}$ for 11 estimates, $0 < \Delta S < 0.97$			2.7 ± 0.1

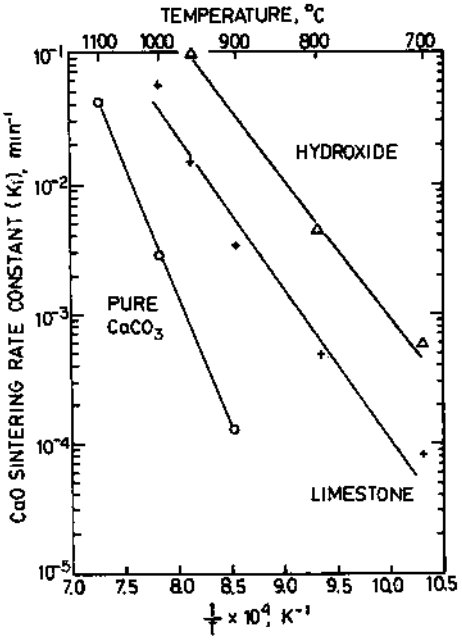

Fig. 4. Effect of temperature and precursor type (hydroxide, limestone or pure $CaCO_3$) on the sintering rate of CaO.

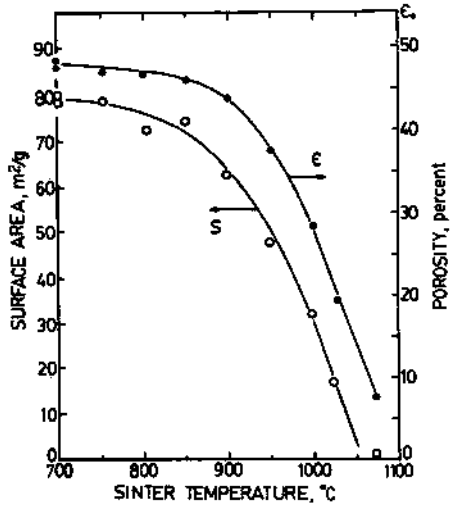

Fig. 5. Porosity and surface area of 2-μm limestone CaO particles after 15-min sinter. Sample size = 250 mg.

the S vs t responses. The lattice defects caused by impurities, especially aliovalent ions, accelerate this solid-state diffusion process (West, 1984). It is clear from Figs 1 and 2 that pure CaO, which lacks these extrinsic defects, sinters more slowly at a given temperature than the impure CaO derived from limestone.

From Fig. 4 it is also apparent that the activation energy for sintering of pure CaO is greater than that of the impure material—a result that is again consistent with the lattice diffusion mechanism. This is explained by the fact that the rate of diffusion is dependent on the concentration of two types of defects, only one of which is present in a pure material: the intrinsic defects induced by temperature. The concentration of intrinsic defects declines exponentially as the temperature is reduced. Impure material, on the other hand, has both the intrinsic defects and extrinsic defects caused by foreign ions in its lattice. The latter are present in constant concentration and thus predominate at low temperature where they effectively reduce the activation energy (Catlow, 1983). According to this interpretation, the two lines should intersect at some higher temperature where intrinsic defects predominate in both materials and their slopes will then be equal (Tilley, 1987). Although single straight lines are shown in Fig. 4, the limestone data suggest that a continuous reduction in slope and activation energy as the temperature is lowered.

The apparent activation energy for the hydroxides is similar to that of the limestone, but the rate constant is an order of magnitude greater at a given temperature. Although the two hydroxides showed no difference in sintering characteristics, neither material was pure by strict standards. Their impurities may partly account for a faster sintering rate relative to the carbonates, but their lower initial porosity is probably the main cause. The theoretical porosity of CaO

derived from $Ca(OH)_2$ is 0.49 based on the change in molar volume. The measured porosity was 0.40, compared to 0.48 for CaO derived from limestone (theoretical $=0.54$). It is reasonable to expect that a denser structure would have more points of contact between grains and therefore sinter faster at any given value of S.

Turning to other matters, the results provide additional evidence in support of the hypothesis that the gas–solid reactions of CaO discussed earlier also involve lattice diffusion. This evidence is the similar effects of impurities and temperature. The diffusion that occurs during sintering and the product-layer diffusion that occurs during reaction are both highly sensitive to temperature and both are strongly affected by impurities. Addition of 5 wt % Na_2SO_4, for example, reduces S by half when limestone particles are calcined and sintered at 800°C for 10 min. It also increases the sulfation rate of presintered CaO by a factor of 10 at that temperature (Borgwardt *et al.*, 1987).

Pore structure development and porosity reduction

When a crystal of $CaCO_3$ or $Ca(OH)_2$ decomposes thermally, the resulting CaO grains, assumed to be nonporous, occupy a total volume approximately equal to the precursor crystal (Hartman *et al.*, 1978). The results of the surface-area-reduction measurements of this study imply that the initial CaO grain structure can be mathematically represented as an assemblage of uniform spheres. This array and the subsequent changes within it are similar to those described by Caillet and Harrison (1972) for MnO sintering except that additional effects occurring on a larger scale must be considered here.

Assuming six points of contact for each grain, the theoretical porosity of such an open-packed array would be 47.6%—in agreement with the measured value for $CaCO_3$ decomposition (Fig. 5). At this stage, before sintering begins, both surface area and porosity have their maximum values, S_o and ε_o. The maximum value of the surface area, 104 m^2/g for $CaCO_3$ decomposition, corresponds to an initial CaO grain diameter of

$$d_g = \frac{6}{S_o \rho_t}$$

or 174 Å for uniform spheres with no connecting necks. The voids enclosed by the array of grains represent the initial micropore structure which would be expected to have an apparent pore diameter of about 40 Å.

As sintering begins, necks develop and grow at each point of contact between grains. In addition to the reduction of surface area, neck growth will result in contraction of the distance between grain centers due to the displacement of matter by lattice diffusion. The grain array thus shrinks and the total volume of micropores between grains is reduced. If the grain array remained continuous throughout the particle, the particle volume would also shrink and porosity should decline simultaneously with surface area.

The results of this study show that surface area undergoes a large reduction before the onset of particle shrinkage. During this initial stage of sintering, the surface area declined from 104 to 80 m^2/g (for carbonate-derived CaO) while the porosity remained nearly constant. One can thus infer that the contracting grain arrays are not continuous throughout the particle, but occur in clusters. The development and contraction of grain clusters within the particle opens a network of macropores between clusters. The presence of the macropore network is revealed by the pore size measurements that show a predominant diameter of 170 Å when the initial sintering stage is completed.

The proposed structure during the initial stage of sintering, involving random clustering of grains with formation of micropores and a macropore network during neck growth, is consistent with the aggregates of "truncated spheres" which Linder and Simonsson (1981) found most applicable to the representation of the initial solid structure of CaO for evaluation of sulfation models. It is also consistent with the pore-tree model of CaO proposed by Simons and Garman (1986) where micropores are "leaves," and macropores are "branches and trunks."

To account for large reductions of surface area, the clusters must contain many grains and/or undergo progressive reclustering. Each cluster would have to contain, for example, 125 of the original grains and fuse completely into a single solid sphere in order to reduce the specific surface area by 80%. The measured diameter of the macropores, 170 Å following the initial stage of sintering, is in accord with this number of grains per average cluster. Since the observed ΔS exceeds 90% at high temperatures, one can conclude that once the micrograins within a cluster have coalesced, accretion and growth of the larger masses continues. This growth presumably involves the formation of new necks between the larger masses and may explain the approximate validity of eq. (1) beyond $\Delta S = 0.5$.

After grain clusters contract and the micropores disappear, the accretion of fused clusters begins, marking the intermediate stage of sintering. During this stage, macropores are also eliminated causing the overall dimensions of the particle to shrink and porosity to decline. The data of Fig. 5 show that the rate of porosity reduction becomes appreciable above 900°C in a nitrogen atmosphere. Equations which predict the rate of change of porosity have been reviewed by Exner and Petzow (1980). The most widely accepted model is Coble's (1961) logarithmic law which accounts for the transport of matter by diffusion and also accounts for a continuous growth in grain size:

$$\varepsilon_o - \varepsilon = k_p \ln (t/t_i) \qquad (2)$$

where ε is the porosity at time t, and k_p contains the

physical constants of diffusion. ε_o and t_i are the porosity and time when particle shrinkage begins.

Equation (2) can be applied to the nascent CaO data if one assumes that the porosity at a given value of S is the same as that indicated by Fig. 5. With this assumption, the data read from Figs 2 and 5 are plotted in Fig. 6 which shows satisfactory agreement with the Coble model within the uncertainties of the $S(t, T)$ measurements. The induction period, t_i, distinguishes the initial stage from the intermediate stage of sintering; it can be delineated by extrapolating ε to the theoretical porosity at the instant of $CaCO_3$ decomposition, $\varepsilon_o = 0.54$. t_i includes the time required to heat up from the 700°C calcination temperature to the sintering temperature plus the time elapsed during cluster coalescence and macropore development prior to the onset of particle shrinkage. Figure 6 shows that an induction period of 3 min elapses before porosity reduction begins at 950°C, thus marking the beginning of the intermediate stage at that temperature. From Fig. 2, the surface area decreases from 104 to 80 m^2/g during the 3-min initial stage of sintering in which micropores are eliminated and macropores expand with a constant overall porosity of ε_o.

There is substantial discrepancy between the value of S_o determined from 25-mg samples (104 m^2/g, Table 1) and the maximum S obtained with the 250-mg samples (79 m^2/g, Fig. 9) used for porosity measurements. The difference is attributed to the effect of CO_2 evolved during calcination which accelerates CaO sintering (Beruto *et al.*, 1984; Borgwardt *et al.*, 1986). That effect will be pronounced in a large mass of particles, especially when the gas flowing through it is subject to channeling. Maximum initial surface is attained when the particles are well dispersed in a high-velocity gas stream during decomposition—conditions that require small sample size.

SUMMARY AND CONCLUSIONS

Sintering rates of CaO derived from limestone were measured in an inert atmosphere, i.e. at conditions not complicated by the catalytic effects of CO_2 and H_2O. The observed responses are consistent with a structural model in which the nascent CaO forms an open packed array of spherical grains, initially 174 Å diameter, that interact by neck formation and neck growth at their points of contact. The reduction of surface area results from transfer of matter during neck growth and grain fusion. The initial stage of sintering is characterized by development of micropores within grain clusters and a macropore network between clusters. The sintering rate increases rapidly with temperature; it is also accelerated by the presence of impurities in the CaO. The intermediate stage is characterized by reduction of porosity which begins when fused clusters coalesce, eliminating macropores.

CaO derived from $Ca(OH)_2$ sintered faster than carbonate derivatives, but the surface reduction in both materials during the initial and intermediate stages were consistent with the model of neck growth kinetics formulated by German and Munir. The data analysis indicates that transport of matter occurs by the lattice diffusion mechanism. This conclusion is supported by measurements of sintering rates of ultra pure CaO which are much slower, especially at low temperatures where impurity-induced lattice defects most strongly affect solid-state diffusion. The similar effects of temperature and impurities on CaO sintering and on the product-layer diffusivity of the CaO sulfation reaction are evidence linking the transport mechanism of these two processes.

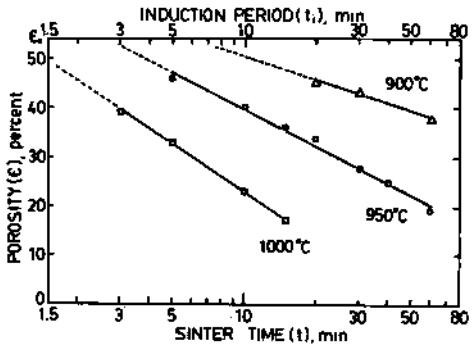

Fig. 6. Inferred porosity reduction in nascent CaO.

NOTATION

D	coefficient of diffusivity, l^2/t
D_o	Arrhenius frequency factor, l^2/t
d_g	initial grain diameter, l
E	activation energy of diffusion, cal/mol
K_i	sintering rate constant in an inert atmosphere, t^{-1}
k_p	particle shrinkage constant defined by eq. (2)
R	gas constant
S	specific surface area at time t, l^2/m
S_o	initial specific surface area of CaO following decomposition of its precursor, l^2/m
ΔS	total change in specific surface area, l^2/m
t	time, t
t_i	induction period for onset of particle shrinkage
T	temperature, K

Greek letters

γ	mechanism-dependent exponent defined by eq. (1)
ε	particle porosity at time t
ε_o	initial particle porosity following decomposition of CaO precursor
ρ_t	true density of CaO, m/l^3

REFERENCES

Beittel, R., Gooch, J. P., Dismukes, E. B. and Muzio, L. J., 1985, Studies of sorbent calcination and SO_2-sorbent reactions in a pilot-scale furnace, in *Proceedings: First Joint Symposium on Dry SO_2 and Simultaneous SO_2/NO_x Control Technologies*, Vol. 1, 16.1. EPA-600/9-85-020a (NTIS PB85-232353)

Beruto, D., Barco, L. and Searcy, A. W., 1984, CO_2—catalyzed surface area and porosity changes in high surface area CaO aggregates. *J. Am. Ceram. Soc.* **67**, 512–515.

Bhatia, S. K. and Perlmutter, D. D., 1981, The effect of pore structure on fluid–solid reactions: application to the SO_2–lime reaction. *A.I.Ch.E. J.* **32**, 226–234.

Bhatia, S. K. and Perlmutter, D. D., 1983, Effect of the product layer on the kinetics of the CO_2–lime reaction. *A.I.Ch.E. J.* **29**, 79–86.

Borgwardt, R. H., 1985, Calcination kinetics and surface area of dispersed limestone particles. *A.I.Ch.E. J.* **31**, 103–111.

Borgwardt, R. H. and Bruce, K. R., 1986, Effect of specific surface area on the reactivity of CaO with SO_2. *A.I.Ch.E. J.* **32**, 239–246.

Borgwardt, R. H., Bruce, K. R. and Blake, J., 1987, An investigation of product-layer diffusivity for CaO sulfation. *Ind. Engng Chem. Res.* **26**, 1993–1998.

Borgwardt, R. H., Roache, N. F. and Bruce, K. R., 1984, Surface area of calcium oxide and kinetics of calcium sulfide formation. *Envir. Prog.* **3**, 129–135.

Borgwardt, R. H., Roache, N. F. and Bruce, K. R., 1986, Method for variation of grain size in studies of gas–solid reactions involving CaO. *Ind. Engng Chem. Fundam.* **25**, 165–169.

Caillet, D. A. and Harrison, D. P., 1982, Structural property variations in the MnO–MnS system. *Chem. Engng Sci.* **37**, 635–636.

Catlow, C. R. A., 1983, in *Mass Transport in Solids* (Edited by F. Beniere and C. R. A. Catlow), pp. 10–11. Plenum Press, New York.

Coble R. L., 1961, Sintering in crystalline solids, II. Experimental test of diffusion models. *J. appl. Phys.* **32**, 793–799.

Cole, J. A., Kramlich, J. C., Seeker, W. R. and Heap, M. P., 1985, Activation and reactivity of calcareous sorbents toward sulfur dioxide. *Envir. Sci. Technol.* **13**, 1065–1072.

Exner, H. E. and Petzow, G., 1980, A critical evaluation of shrinkage equations, in *Sintering Processes* (Edited by G. C. Kuczynski), pp. 107–120. Plenum Press, New York.

German, R. M. and Munir, Z. A., 1976, Surface area reduction during isothermal sintering. *J. Am. Ceram. Soc.* **59**, 379–383.

Hartman, M., Pata, J. and Coughlin, R. W., 1978, Influence of porosity of calcium carbonates on their reactivity with sulfur dioxide. *Ind. Engng Process Des. Dev.* **17**, 411–419.

Harvey, R. D., 1971, Petrographic and mineralogical characteristics of carbonate rocks related to sulfur dioxide sorption in flue gases. (EPA) APTD-0920 (NTIS PB206-487).

Johnson, D. L., 1980, Solid state sintering models, in *Sintering Processes* (Edited by G. C. Kuczynski), pp. 97–120. Plenum Press, New York.

Lachapelle, D. G., 1985, EPA's LIMB technology development program. *Chem. Engng Prog.* **81**, 52–65.

Lindner, B. and Simonsson, D., 1981, Comparison of structural models for gas–solid reactions in porous solids undergoing structural changes. *Chem. Engng Sci.* **35**, 1519–1527.

Rhines, F. N. and DeHoff, R. T., 1984, Channel network decay in sintering, in *Sintering and Heterogeneous Catalysis* (Edited by G. C. Kuczynski), pp. 49–61. Plenum Press, New York.

Simons, G. A. and Garman, A. R., 1986, Small pore closure and the deactivation of the limestone sulfation reaction. *A.I.Ch.E. J.* **32**, 1491–1499.

Slaughter, D. M., Chen, S. L. and Seeker, W. R., 1986, Enhanced sulfur capture by promoted calcium-based sorbents, in *Proceedings*: 1986 *Joint Symposium on Dry* SO_2 *and Simultaneous* SO_2/NO_x *Control Technologies*, Vol. 1, 12.1 EPA-600/9-86-029a (NTIS PB87-120465).

Sotirchos, S. V. and Yu, H. C., 1985, Mathematical modelling of gas–solid reactions with solid product. *Chem. Engng Sci.* **40**, 2039–2052.

Tilley, R. J. D., 1987, *Defect Crystal Chemistry*, pp. 27 and 54. Chapman & Hall, New York.

West, A. R., 1984, *Solid State Chemistry and its Applications*, p. 328. John Wiley, New York.